EPJ Web of Conferences **163**, 00063 (2017) DOI: 10.1051/epjconf/201716300063
FUSION17

Near-barrier Fusion Evaporation and Fission of ^{28}Si+^{174}Yb and ^{32}S+^{170}Er

Dongxi Wang[1], *Chengjian* Lin[1,2,⋆], *Huiming* Jia[1], *Nanru* Ma[1], *Lijie* Sun[1], *Xinxing* Xu[1,3], *Lei* Yang[1], *Feng* Yang[1], *Huanqiao* Zhang[1], and *Pengfei* Bao[1]

[1] *China Institute of Atomic Energy, P.O. Box 275(10), Beijing 102413, China*
[2] *College of Physics and Technology, Guangxi Normal University, Guilin 541004, China*
[3] *Department of Physics, The University of Hong Kong, Hong Kong, China.*

Abstract. Fusion evaporation residues and fission fragments have been measured, respectively, at energies around the Coulomb barrier for the ^{28}Si+^{174}Yb and ^{32}S+^{170}Er systems forming the same compound nucleus ^{202}Po. The excitation function of fusion evaporation, fission as well as capture reactions were deduced. Coupled-channels analyses reveal that couplings to the deformations of targets and the two-phonon states of projectiles contribute much to the enhancement of capture cross sections at sub-barrier energies. The mass and total kinetic energy of fission fragments were deduced by the time-difference method assuming full momentum transfer in a two-body kinematics. The mass-energy and mass-angle distributions were obtained and no obvious quasi-fission components were observed in this bombarding energy range. Further, mass distributions of fission fragments were fitted to extract their widths. Results show that the mass widths decrease monotonically with decreasing energy, but might start to increase when $E_{\rm c.m.}/V_{\rm B} < 0.95$ for both systems.

1 Introduction

Heavy-ion induced fusion-fission reactions at energies around the Coulomb barrier have attracted much attention [1, 2], due to many degrees of freedom involved in the interaction processes. It has been experimentally proved that the coupled interactions of some intrinsic motions and relative motion play a significant role in the process that two nuclei fuse into one, and it is commonly interpreted theoretically as coupled-channels (CC) effects. It is expected that the deformation [3], vibrational state [4] and transfer channel [5–7] may be involved in the capture reaction. After two nuclei come into contact with each other, the system evolves along the potential energy surface, the path of which may be complicated. The system may achieve equilibrium of all the degrees of freedom and whereafter the compound nucleus (CN) can survive through evaporating light particles. The system can also go to fission via some equilibrium or non-equilibrium processes, such as complete fusion-fission, pre-equilibrium fission [8], quasi-fission [9] and fast fission [10–12]. These processes may strongly depend on some factors of the entrance channel, for example, deformations of projectile and target, the mass asymmetry, and so on. Comprehensive research on fusion-fission reactions can cast useful light on the understanding of heavy ion induced reactions.

Previously, we have measured the angular distributions for the fission fragments of the ^{32}S+^{184}W system [13] and, the mass and energy distributions for the fission fragments of the ^{34}S+^{186}W system [14]. Anisotropy deduced from the measured angular distributions reveals the appearance of non-equilibrium fission. It can be interpreted as quasi-fission by the dinuclear system model or pre-equilibrium fission [14]. In order to further explore on the fission mechanism, study on extensive systems is desired.

In the present work, the ^{28}Si+^{174}Yb and ^{32}S+^{170}Er systems were chosen because both systems form the same compound nucleus ^{202}Po. It is noted that mass-angle correlations and mass ratio distributions of fission fragments have been measured systematically for the systems of ^{16}O+^{186}Os, ^{24}Mg+^{178}Hf, ^{34}S+^{168}Er, and ^{48}Ti+^{154}Sm [15], also forming the same compound nucleus ^{202}Po. Therefore, the entrance-channel dependence can be investigated in a systematic manner. Moreover, both fusion evaporation residues (ERs) and fission fragments have been measured for the ^{34}S+^{168}Er system [16], giving a good reference to the present work. It is worth to point out that both fusion evaporation and fission have observable cross sections at near-barrier energy region due to the higher fission barrier of ^{202}Po ($\approx$ 15 MeV) [17]. It provides a good case to explore the evolving paths of both fusion and fission along the potential energy surface, to strictly test as well as help to develop relevant theoretical models, and to comprehensively understand the complete fusion-fission dynamics.

In the following Sec. 2, details of the experimental procedure for fusion evaporation and fission measurements are present. Experimental results and preliminary discussions are reported in Sec. 3 and conclusions are given in Sec. 4 finally.

⋆e-mail: cjlin@ciae.ac.cn

2 Experimental procedure

The beams of ^{32}S and ^{28}Si, at several energies in the range of 133.0 - 181.0 MeV and 119.2 - 162.1 MeV, respectively, were supplied by the HI-13 tandem accelerator of the China Institute of Atomic Energy, Beijing, China. Highly isotopically-enriched $^{170}ErO_3$ (95 μg/cm^2) and ^{174}Yb (130 μg/cm^2) targets sputtered onto carbon backings (20-23 μg/cm^2) were used. Four silicon (Si) detectors placed symmetrically at $\theta_{lab} = \pm 20^\circ$ (right-left and up-down) with respect to the beam direction were used to monitor the Rutherford scattering and to provide a normalization for the fusion evaporation and fission cross sections. Fusion ERs and fission fragments were measured independently with the same beam.

2.1 Measurement of fusion ERs

Fusion ERs mainly concentrated within a few degrees of the incident beam direction were separated from the beam-like particles (BLPs) by using an electrostatic deflector setup [18]. It consists of two pairs of electrodes followed by two micro-channel plate (MCP) detectors and a 48×48 mm^2 quadrant Si detector. Distances of MCP1-MCP2 and MCP2-Si are 41.0 and 22.7 cm, respectively. Time-of-flight (ToF) versus E spectra, ToF1-E and ToF2-E, are useful to reduce the spurious backgrounds from the random coincidences between the Si and one of the MCPs, especially for the measurements of low fusion evaporation cross sections at sub-barrier energies and for asymmetric systems studied in this work. The reaction products were limited by a collimator of 2.5 mm in diameter before entering the electric fields, corresponding to an opening angle $\theta_{lab} = \pm 0.38^\circ$. Fig. 1 shows a typical ToF1 versus E spectrum for the ^{32}S+^{170}Er system at an energy near the Coulomb barrier, where BLPs and ERs can be separated clearly.

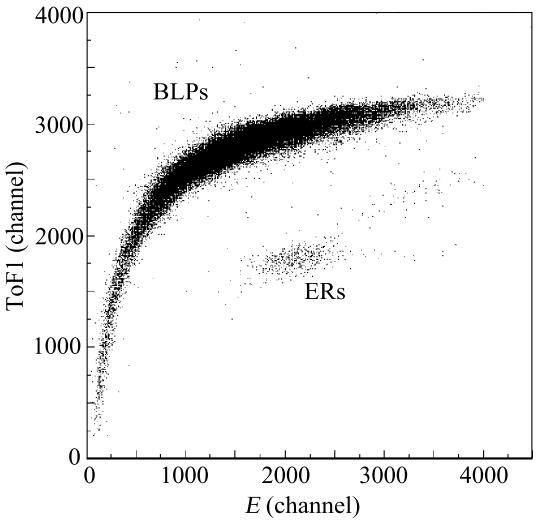

Figure 1. Two-dimensional plot ToF1-E taken at E_{lab} = 169 MeV and $\theta_{lab} = 2^\circ$ for ^{32}S+^{170}Er. A group of BLPs and ERs are indicated.

The ERs angular distributions were measured in the range $\theta_{lab} = -4^\circ$ to $+8^\circ$ with a step of 0.5° or 1° for both systems at E_{lab} = 143 MeV and 163 MeV, respectively. Their shapes do not change appreciably with the beam energy, resulting from the dominant neutron and/or proton evaporation from the CN [19], which is consistent with the calculation of the code PACE2 [20]. Typical angular distributions of ERs for the ^{32}S+^{170}Er system as well as their fittings by a single Gaussian function are shown in Fig. 2.

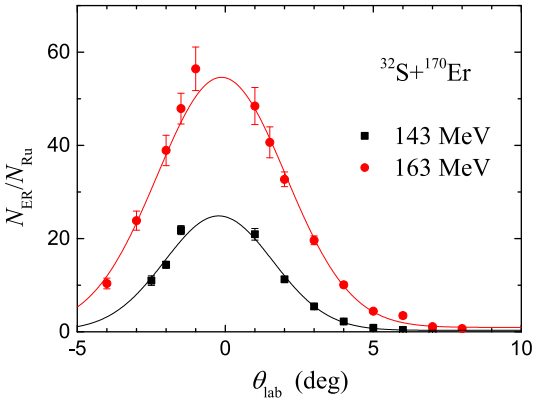

Figure 2. Angular distributions of ERs for the ^{32}S+^{170}Er system at E_{lab} = 143 MeV and 163 MeV. Curves are single Gaussian fits used to obtain the total fusion evaporation cross sections.

For other energies, ERs were measured only at $\theta_{lab} = 1.5^\circ$. Total fusion evaporation cross sections were obtained by integration of the angular distribution with the same shape. Meanwhile, corrections were made for the transmission efficiency of the electrostatic deflector, which is about 40%.

2.2 Measurement of fission fragments

Two fission fragments were detected in coincidence by using two Parallel Plate Avalanche Counters (PPACs). The PPAC1 and PPAC2 have an active area ($X\times Y$) of 180×100 mm^2 and 250×100 mm^2 with X and Y position resolution of about 1 and 2 mm, respectively. The emission angles θ_1 and θ_2 projected on the reaction $X-Z$ plane and the out-of-plane angles φ_1 and φ_2 for the fission fragment 1 and 2 were transformed from the XYZ coordinate, assuming the beam direaction as the Z axis. The detectors were located around the target, centering at $\theta_1 = 45^\circ$ and $\theta_2 = -105^\circ$ with distances of d_1 = 155 mm and d_2 = 125 mm from the target to the centers of entrance windows and covered angles of $\Delta\theta_1 = \pm27^\circ$ and $\Delta\theta_2 = \pm30^\circ$ as well as $14.9^\circ \le \varphi_1 \le 75.7^\circ$ and $60.0^\circ \le \varphi_2 \le 150.0^\circ$ for PPAC1 and PPAC2, respectively. The detectors were operated with isobutane gas at a pressure of about 3 Torr.

The time difference ΔT between the two fission fragments was measured with start and stop signals obtained from PPAC2 and PPAC1, along with the energy losses ΔE_1 and ΔE_2 in both PPACs by passing nuclei. Fig. 3 (a) gives an example of measured coincident events in the

ΔE_1+ΔE_2 versus ΔT coordinate plane, for ^{28}Si+^{174}Yb reactions at the $E_{\rm c.m.}/V_{\rm B}$ = 1.25. A clear separation between fission fragments and scattered particles can be noted.

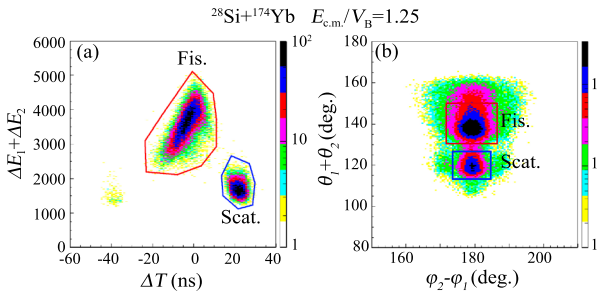

Figure 3. (a) Events from the ^{28}Si+^{174}Yb reaction, mapped on the ΔE_1+ΔE_2 versus ΔT axes. Fission events within the polygon and scattering events are clearly separated. (b) Same as in (a) but in the coordinates of $\theta_1 + \theta_2$ versus $\varphi_2 - \varphi_1$.

An additional way to distinguish fission fragments from the scattered projectile and recoiled nuclei is to exploit the difference in the reaction kinematics. This is demonstrated in Fig. 3 (b), where events are plotted in the $\theta_1 + \theta_2$ versus $\varphi_2 - \varphi_1$ coordinate plane. The calibration for the time difference ΔT was made from the elastic-recoil peak positions appearing in the ΔT spectrum. The timing resolution of a single PPAC pixel was determined to be 0.3 ns. The experimental mass resolution obtained from the elastic scattering peak is about $\sigma_{\rm exp} = 2 - 4$ u, depending on the measured angle.

In the present work, the ΔT method was employed to deduce the velocity and mass of fission fragment by applying the momentum conservation as well as the mass conservation in a two-body kinematics. In the laboratory system, we have

$$m_1 v_1 sin\theta_1 = m_2 v_2 sin\theta_2, \quad (1)$$

$$m_1 v_1 cos\theta_1 + m_2 v_2 cos\theta_2 = m_{\rm P} v_{\rm P} = m_{\rm CN} v_{\rm CN}, \quad (2)$$

$$m_1 + m_2 = m_{\rm P} + m_{\rm T} = m_{\rm CN}, \quad (3)$$

$$\Delta T = \frac{r_1}{v_1} - \frac{r_2}{v_2}, \quad (4)$$

where m is the mass, v is the velocity and r is the flight distance of outgoing particles before being detected, subscript P, T, CN and 1, 2 represent the projectile, target, CN and fission fragments, respectively. Finally, the velocity and mass of outgoing particles can be expressed as

$$v_1 = \frac{r_1 sin\theta_1 + r_2 sin\theta_2}{r_2 sin(\theta_1 + \theta_2) + \Delta T v_{\rm CN} sin\theta_1} \cdot v_{\rm CN}, \quad (5)$$

$$v_2 = \frac{r_1 sin\theta_1 + r_2 sin\theta_2}{r_1 sin(\theta_1 + \theta_2) - \Delta T v_{\rm CN} sin\theta_2} \cdot v_{\rm CN}, \quad (6)$$

$$m_1 = \frac{r_2 sin(\theta_1 + \theta_2) + \Delta T v_{\rm CN} sin\theta_1}{r_1 sin\theta_1 + r_2 sin\theta_2} \cdot \frac{sin\theta_2}{sin(\theta_1 + \theta_2)} \cdot m_{\rm CN}, \quad (7)$$

$$m_2 = \frac{r_1 sin(\theta_1 + \theta_2) - \Delta T v_{\rm CN} sin\theta_2}{r_1 sin\theta_1 + r_2 sin\theta_2} \cdot \frac{sin\theta_2}{sin(\theta_1 + \theta_2)} \cdot m_{\rm CN}, \quad (8)$$

and then the total kinetic energy (TKE) can be calculated,

$$\mathrm{TKE} = \frac{1}{2} m_1 v_1^2 + \frac{1}{2} m_2 v_2^2. \quad (9)$$

Table 1. The relevant parameters used in the CCFULL calculations.

Nuclei	E_{2^+} (MeV)	B($E2$) (W.u.)	β_2
^{28}Si	1.779	13.2	−0.411
^{32}S	2.230	10.1	0.315
^{170}Er	0.079	208	0.336
^{174}Yb	0.076	201	0.321

3 Results and discussions

3.1 Excitation function

The excitation functions of evaporation were determined by doing the integrals with respect to angular distribution and performing the correction of the transmission efficiency. As for fission, position and time difference of fission fragments detected by PPACs were used to deduce their mass, emission angle and TKE. Integral of the angular distribution leads to the fission cross section, and the fission excitation function was then determined. Adding the excitation functions of ERs and fission together, the excitation function of capture reaction was obtained.

The measured fusion ERs, fission and capture excitation functions are shown in Fig. 4 for ^{28}Si+^{174}Yb and ^{32}S+^{170}Er, respectively. The CC code CCFULL [21] was used to reproduce the capture cross sections and the relevant parameters used in the CC calculations are listed in Table 1. It can be seen from the figure that the single-channel (SC) results (dashed lines) under-predict the sub-barrier data. However, experimental capture excitation functions could generally reproduced by the CC calculations with couplings to the vibrational two-phonon 2^+ states of projectiles and the rotational $2^+, 4^+, 6^+, 8^+$ states of targets, except a small deviation at energies around the barrier.

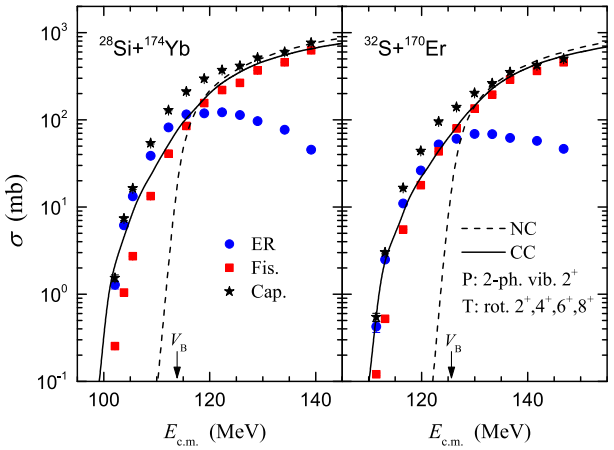

Figure 4. Experimental cross-sections of fusion evaporation (circle), fission (square) and capture (star) for the ^{28}Si+^{174}Yb (left panel) and ^{32}S+^{170}Er (right panel) systems, together with the CC (solid curve) and the SC (dashed curve) calculation results.

3.2 Mass-TKE correlations

The contour diagrams representing the angle integrated fragment mass-TKE correlations for a selected subset of the ^{28}Si+^{174}Yb and ^{32}S+^{170}Er systems are shown in Fig. 5. In both figures, one can distinguish two regions of a scattering region close to the target and projectile masses and a region of fission in the direction of symmetry. The almost independence of the fission TKE on the bombarding energy indicates that the initial excess kinetic energy is completely damped out and transformed into internal excitation in all capture processes.

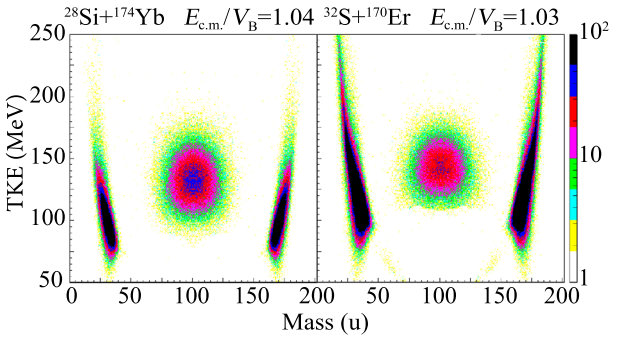

Figure 5. The correlations between fragment mass and TKE for the reactions of ^{28}Si+^{174}Yb (left) and ^{32}S+^{170}Er (right) at $E_{c.m.}/V_B$ = 1.04 and 1.03, respectively.

3.3 Mass-angle correlations

The correlations between fragment mass and center-of-mass angle for the ^{28}Si+^{174}Yb and ^{32}S+^{170}Er systems are shown as contour diagrams in Fig. 6. Also in these diagrams, the separation between scattering and fission reactions is clearly apparent. Both the two systems show symmetric fission fragment mass distributions at all angles, which is a characteristic feature for the CN fission.

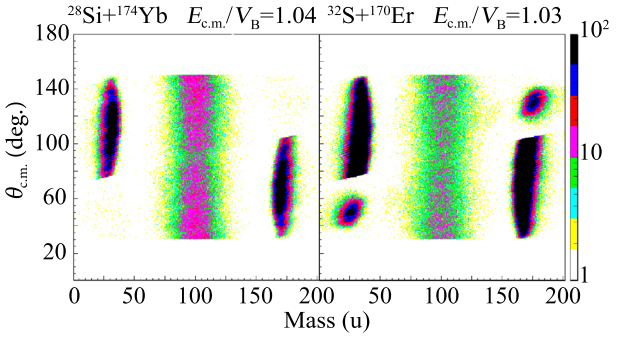

Figure 6. The correlations between fragment mass and $\theta_{c.m.}$ for the reactions of ^{28}Si+^{174}Yb (left) and ^{32}S+^{170}Er (right) at $E_{c.m.}/V_B$ = 1.04 and 1.03, respectively.

3.4 Mass distributions

As mentioned above, no obvious correlations were observed in mass-angle and mass-TKE distributions for the two systems at energies around the barrier. The existing systematic study shows that the width of mass distribution for the quasi-fission is larger than that for the fusion-fission [22]. Therefore an increased mass width can be used as an indicator for the presence of quasi-fission. Fig. 7 shows the mass distributions of fission fragments for the ^{28}Si+^{174}Yb and ^{32}S+^{170}Er systems at three reaction energies, respectively, where the fission yields are normalized to 200%.

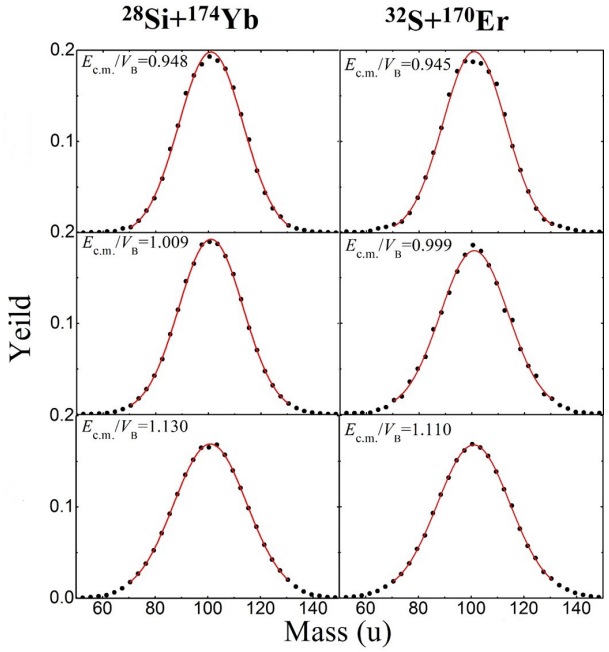

Figure 7. Mass distributions of fission fragments for the reactions of ^{28}Si+^{174}Yb (left) and ^{32}S+^{170}Er (right) at different reaction energies.

The mass spectra can be described by a single Gaussian distribution with the center at $A_{CN}/2$. The standard deviation σ_M of the mass distributions was obtained at each reaction energy, as shown in Fig. 8. It is evident from the figure that σ_M decreases monotonically with decreasing energy, but seems to increase when $E_{c.m.}/V_B < 0.95$ for both systems.

4 Conclusions

The fusion evaporation and fission reactions of ^{32}S+^{170}Er and ^{28}Si+^{174}Yb were measured at the energy ranges of $0.91 \leq E_{c.m.}/V_B \leq 1.23$ and $0.93 \leq E_{c.m.}/V_B \leq 1.25$, respectively. The excitation functions of fusion evaporation, fission as well as capture reactions were obtained. The coupled-channels calculations, where both the 2^+ two-phonon vibrational-states of projectiles and the 2^+, 4^+, 6^+, 8^+ rotational-states of targets are considered, could roughly reproduce the capture excitation functions for the two systems. For fission, the mass-TKE and mass-angle distributions were deduced and no obvious quasi-fission components were observed in this bombarding energy range. The mass widths decrease monotonically with decreasing energy, but might start to increase when

$E_{\mathrm{c.m.}}/V_{\mathrm{B}} < 0.95$ for both systems. Further study is still in progress.

5 Acknowledgments

This work is supported by the National Key Basic Research Program of China (Grant No. 2013CB834404) and by the National Natural Science Foundation of China (Grants No. 11635015, No. 11375268, No. 11475263, No. U1432246, No. U1432127, and No. 11505293).

References

[1] K. Banerjee *et al*, Phys. Rev. C **83**, 024605 (2011).
[2] D.J. Hinde *et al*, Phys. Rev. Lett. **89**, 282701 (2002).
[3] C. Y. Wong, Phys. Rev. Lett. **31**, 766 (1973).
[4] H. Esbensen, Nucl. Phys. A **352**, 147 (1981).
[5] R. A. Broglia *et al*, Phys. Lett. B **133**, 34 (1983).
[6] C. H. Dasso *et al*, Nucl. Phys. A **407**, 221 (1983).
[7] C. H. Dasso *et al*, Nucl. Phys. A **405**, 381 (1983).
[8] Z. H. Liu *et al*, Phys. Lett. B **353**, 173 (1995).
[9] W. J. Swiatecki *et al*, Phys. Scr. **24**, 113 (1981).
[10] B. Heusch *et al*, Z. Phys. A **288**, 391 (1978).
[11] C. Lebrun *et al*, Nucl. Phys. A **321**, 207 (1979).
[12] C. Gregoire *et al*, Phys. Lett. B **99**, 17 (1981).
[13] H. Q. Zhang *et al*, Phys. Rev. C **81**, 034611 (2010).
[14] C. J. Lin *et al*, J. Phys. Conf. Ser. **420**, 012126 (2013).
[15] R. Rafiei *et al*, Phys. Rev. C **77**, 024606 (2008).
[16] C. R. Morton *et al*, Phys. Rev. C **62**, 024607 (2000).
[17] P. Möller *et al*, Phys. Rev. C **79**, 064304 (2009).
[18] H. Q. Zhang *et al*, Chin. Phys. C **34**, 1628 (2010).
[19] D. J. Hinde *et al*, Nucl. Phys. A **385**, 109 (1982); *ibid.* **398**, 308 (1983).
[20] A. Gavron, Phys. Rev. C **21**, 230 (1980).
[21] K. Hagino *et al*, Comput. Phys. Commun. **123**, 143 (1999).
[22] C. J. Lin *et al*, Phys. Rev. C **85**, 014611 (2012).

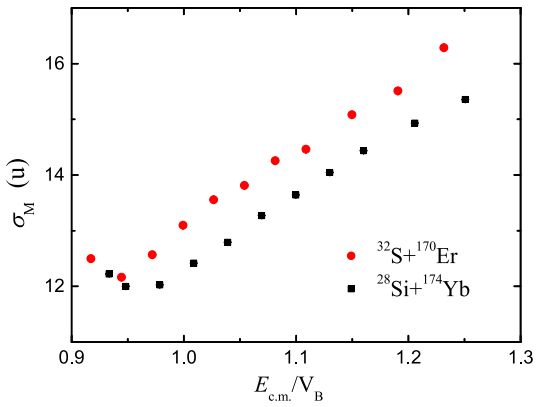

Figure 8. Mass widths of fission fragments as a function of $E_{\mathrm{c.m.}}/V_{\mathrm{B}}$ for the ^{32}S+^{170}Er (circle) and ^{28}Si+^{174}Yb (square) systems.